https://doi.org/10.22226/2410-3535-2022-4-486-492

Features of phase formation of pyrochlore-type $Bi_2Cr_{1/6}Mn_{1/6}Fe_{1/6}Co_{1/6}Ni_{1/6}Cu_{1/6}Ta_2O_{9+\Delta}$

E. P. Rylchenko†,1, B. A. Makeev2, D. V. Sivkov3, R. I. Korolev1, N. A. Zhuk1

†rlena12@mail.ru

[1]Syktyvkar State University, Syktyvkar, 167001, Russia
[2]Institute of Geology of the Komi Science Center UB RAS, Syktyvkar, 167982, Russia
[3]Institute of Physics and Mathematics of the Komi Science Center UB RAS, Syktyvkar, Republic of Komi, 167982, Russia

The study of the process of phase formation of multicomponent pyrochlore ($Bi_{2-x}Cr_{1/6}Mn_{1/6}Fe_{1/6}Co_{1/6}Ni_{1/6}Cu_{1/6}Ta_2O_{9+\Delta}$) in the course of solid-phase synthesis showed that the precursor of the pyrochlore phase is bismuth orthotantalate. Of all the precursors, cobalt and nickel oxides are the last to enter the chemical reaction (at 850 – 900°C). Intermediate phases in the course of synthesis are complex oxides $Bi_{16}CrO_{27}$, $Bi_{25}FeO_{40}$, $BiTaO_4$, Bi_3TaO_7, $CoTa_2O_6$. During the evolution of the pyrochlore phase, a nonmonotonic change in the unit cell parameter is observed. Phase-clean pyrochlore is synthesized at a temperature of 1000 –1050°C. Ceramics is characterized by a porous, loose microstructure with an average grain size of 0.5 –1 μm; the porosity of a sample calcined at 1050°C is 19 percent.

Keywords: high-entropy oxides, pyrochlore, bismuth tantalate, doping with transitional 3d-elements.

1. Introduction

Bismuth-containing pyrochlores exhibit a wide range of practically useful properties, among which are dielectric properties (low dielectric losses and high dielectric constant, adjustable temperature coefficient of capacitance), catalytic properties in the UV and visible range [1– 3]. A useful addition is the relatively low synthesis temperature and thermal stability of bismuth pyrochlores [4]. In the crystal structure of pyrochlore $A_2B_2O_6O'$, two interpenetrating and weakly interacting sublattices are distinguished [5, 6]. The cationic sublattice A_2O' is similar to the structure of anticristobalite, the sublattice B_2O_6 forms a three-dimensional framework of vertex-linked octahedrons. Octahedral positions B are occupied by relatively small cations (Ta^{+5}, Ru^{+4}, Zr^{+4}, Sb^{+5}), larger ions (Bi^{+3}, Sm^{+3}, Pb^{+2}) are distributed in eight-coordinated positions A. The flexibility of the pyrochlore crystal structure to cation substitutions in the bismuth/tantalum sublattices and to oxygen vacancies in the A_2O' sublattice makes it possible to control their functional properties [5 –10]. Currently, pyrochlores based on bismuth tantalate and niobate are being actively studied due to their promising dielectric and catalytic properties [7 –15]. A feature of the pyrochlores under consideration is the unfilled bismuth sublattice due to the $6s^2$ electron pair and the ability of transition element ions to simultaneously reside in the cationic sublattices of bismuth (A_2O') and tantalum (niobium) (B_2O_6), causing relaxation processes in ceramics [15 –19]. Studies of pyrochlores based on bismuth tantalate containing 3d transition ions (Cu, Ni, Fe, Cr, Co, Zn) [10 –12,14,17, 21– 23] have shown that porous ceramics are formed with low dielectric losses and moderate values of dielectric permittivity. Copper-containing bismuth tantalates are characterized by a special behavior, which exhibit multiple dielectric relaxation at temperatures above room temperature [20, 21].

As established earlier, monocomponent pyrochlores containing ions of one 3d-element (Cu, Ni, Fe, Cr, Co, Mn) [4,10,11, 20 – 23] exhibit unique properties depending on the nature of the transition element. It is of interest to study the mutual influence of a combination of atoms of transition elements on the physicochemical properties, on the microstructure of multicomponent pyrochlore of the same stoichiometry. In this regard, in the presented work, an attempt was made to synthesize a multicomponent pyrochlore. In this work, the process of phase formation was studied and the optimal conditions for synthesis by the solid-phase method were established. The features of phase formation are revealed, the density and microstructure of ceramics are studied.

2. Experimental

High-entropy pyrochlore was synthesized by the standard ceramic technology from the corresponding Bi (III) (99.5%), Ta (V) (99.99%), Ni (II) (≥99%), Co (II, III) (99.99), Cu (II) (≥99%), Mn (III) (≥99%), Cr (III) (99.00%), Fe (III) (98.70%) oxides. The purity of the reagent is shown in parentheses. The stoichiometric mixture of precursors was finely ground and homogenized in a jasper mortar for one hour. The resulting homogeneous mixture was compacted in the form of disks using a Plexiglas mold. A manual press was used to press the sample. The pressing pressure was 20 Atm. The samples were calcined in air in stages at a temperature of 650, 850,

950, 1050°C for 60 hours. At each stage, the samples were again ground and pressed into tablets. X-ray phase analysis was performed using a Shimadzu 6000 X-ray diffractometer (CuK_α radiation; $2\theta = 10 - 60°$; scanning speed 2.0°/min). The unit cell parameters of pyrochlores were calculated using the CSD software package [24]. The phase formation process was studied using X-ray phase analysis of samples sequentially calcined in the temperature range from 650 to 1050°C (step 50°C) for 15 h at each stage of heat treatment. After each calcination, the sample was carefully homogenized and pressed again in the form of disks to ensure tight contact between the ceramic grains. Surface morphology studies and local quantitative elemental analysis of the samples were performed using a scanning electron microscope (Tescan VEGA 3LMN) and an energy dispersive X-ray spectrometer (INCA Energy 450).

3. Results and discussion

According to X-ray-phase analysis, a sample of the complex composition of $Bi_2Cr_{1/6}Mn_{1/6}Fe_{1/6}Co_{1/6}Ni_{1/6}Cu_{1/6}Ta_2O_{9+\Delta}$ is crystallized in the structural type of pyrochlore (sp. gr. *Fd*-3*m*) and, regardless of the conditions of the synthesis, contains an admixture (7.9 mol.%) orthotantalate of bismuth of the triclinic modification (β-$BiTaO_4$) [25]. In order to obtain phase-pure preparations, samples with a deficiency of atoms in both cationic sublattices of bismuth and tantalum, and separately were synthesized. Meanwhile, absolutely single-phase highly entropic chemicals are reproducibly synthesized in the case of compositions with a deficiency of bismuth atoms in the cationic sublattice, e.g., $Bi_{2-x}Cr_{1/6}Cu_{1/6}Ni_{1/6}Co_{1/6}Fe_{1/6}Mn_{1/6}Ta_2O_{9\pm\Delta}$, $x = 1/3$. The calculation of the unit cell parameter of the $Bi_{2-1/3}Cr_{1/6}Cu_{1/6}Ni_{1/6}Co_{1/6}Fe_{1/6}Mn_{1/6}Ta_2O_{9+\Delta}$ pyrochlore showed the value $a = 10.48106$ Å, which is close to the unit cell parameter of iron-containing pyrochlores based on bismuth tantalate [14, 22]. Figure S1 (supplementary material) shows, that the ceramic microstructure is porous, reticulate, and consists of slightly melted randomly oriented elongated grains of small size 0.5 – 1 μm. In places, crystallites in the form of large agglomerates are observed on the ceramic surface. As microphotographs show, a noticeable fusion of grains is characteristic of ceramics calcined at a temperature of 1050°C.

In order to establish the possibility of influencing the microstructure of ceramics by choosing the optimal conditions for sintering of samples, the stages of phase formation of multicomponent pyrochlore were studied. The process of phase formation was studied by comparing the phase composition of the samples calcined every 50 degrees in the temperature range of 650 – 1050°C. At each stage of calcination, an analysis of the phase composition and microstructure was performed, as well as elemental mapping of the samples. The X-ray diffractions patterns of the calcined preparations are shown in Fig. 1.

It can be seen from the presented X-ray diffraction patterns that the phase composition of the sample significantly depends on the heat treatment temperature. The results of studies of the qualitative composition of the phases in the sample X-ray phase analysis are presented in Table 1. Determination of traces of impurities in the samples was carried out using electron scanning microscopy.

The results of elemental mapping of samples calcined in the range of 650 – 1050°C are shown in Fig. 2 and Fig. S2 (supplementary material). According to the analysis data, the samples calcined at 650°C have the most complex phase composition. Phases of the initial precursors Ta_2O_5, Co_3O_4, NiO and oxide interaction products are identified on the X-ray diffraction pattern — a compound with the sillenite structure $Bi_{25}FeO_{40}$ (sp. gr. *I*23), $Bi_{16}CrO_{27}$ (sp. gr *I*/4*m*), α-$BiTaO_4$ (sp. gr. *Pnna*), Bi_3TaO_7 (sp. gr. *Fm*-3*m*) and the pyrochlore phase [26 – 29]. Elemental mapping of a sample calcined at a temperature of 650°C showed (Fig. 2) that cobalt and nickel are unevenly distributed on its surface, which does not contradict the XRD data (Fig. 3). No other oxides of 3d-element precursors were found as impurity phases, which indicates their entry into chemical interaction. Meanwhile, broadened reflections of the pyrochlore phase are fixed on the X-ray diffraction pattern. Broad reflections indicate the imperfection of the crystal structure, probably due to the nonstoichiometric composition. Apparently, the formation of pyrochlore became possible due to the phase transformation of the α-Bi_2O_3 phase into the more active δ-Bi_2O_3 form [30]. In general, bismuth oxide, as an independent phase, did not appear on X-ray diffraction patterns of samples calcined at 650°C, which indicates its high reactivity and is confirmed by the results of [14]. Part of the tantalum (V) oxide did not enter into the reaction, probably because part of the bismuth (III) oxide was spent on the reaction with iron (III) and chromium (III) oxides to form intermediate products — complex oxides $Bi_{16}CrO_{27}$, $Bi_{25}FeO_{40}$, respectively. Above 700°C, $Bi_{16}CrO_{27}$ is not fixed and, in trace amounts, $Bi_{25}FeO_{40}$ is present, the Bi_3TaO_7 phase disappears. Cobalt and nickel oxide phases are still fixed, as shown by elemental mapping (Fig. S2, supplementary material). As shown by the results of elemental mapping, impurities of nickel and cobalt oxides are not fixed in samples calcined at temperatures above 900°C. With an increase in the calcination temperature, the phase composition of the samples becomes simpler due to the formation of the pyrochlore phase with the participation of intermediate compounds, for example, $BiTaO_4$. A special feature in the process of evolution of the high-entropy pyrochlore phase is the occurrence of an intermediate reaction of the formation of cobalt (nickel) tantalate, which is fixed in samples up to a temperature of 1000°C. We believe that cobalt tantalate was formed, since the position of the reflections on the X-ray diffraction pattern most of all corresponds to this compound. In addition, cobalt oxide is fixed in samples as an impurity up to 900°C. Meanwhile, when studying the phase formation of nickel pyrochlore based on bismuth tantalate, the nickel tantalate phase was not detected [31]. By the way, in [12], when studying the phase formation of copper pyrochlore, an intermediate phase of copper (II) tantalate was recorded, which does not contradict the results of our study. High-temperature treatment of the sample (at temperatures above 800°C) leads to the gradual interaction of $BiTaO_4$ with oxides of nickel, cobalt, cobalt tantalate and the formation of a pyrochlore phase of a given stoichiometry. X-ray diffraction patterns of samples calcined in this temperature range

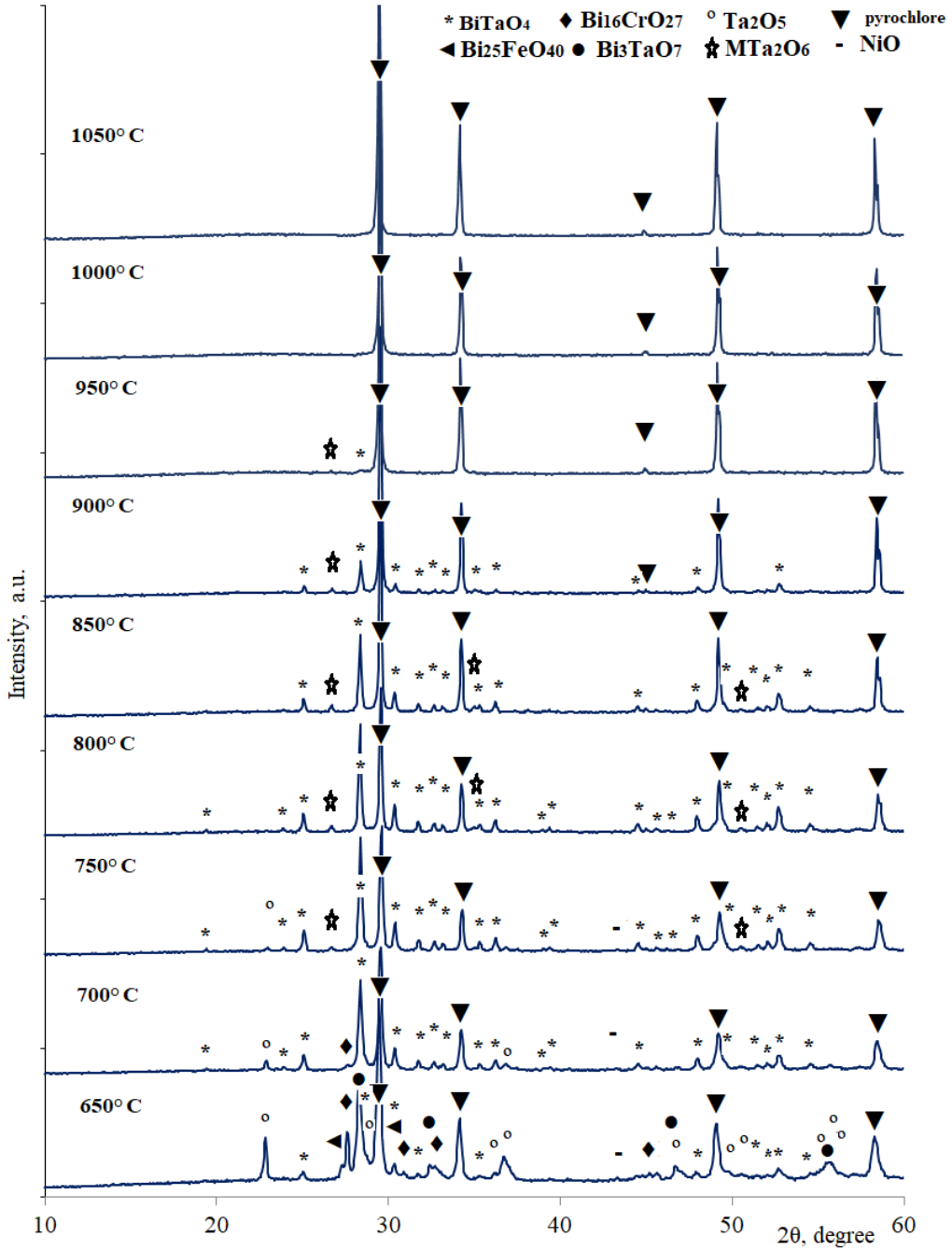

Fig. 1. X-ray diffractions patterns of the $Bi_{2-1/3}Cr_{1/6}Cu_{1/6}Ni_{1/6}Co_{1/6}Fe_{1/6}Mn_{1/6}Ta_2O_{9+\Delta}$ sample, calcined at a temperature from 650 to 1050°C.

Table 1. Phase composition of the $Bi_{2-1/3}Cr_{1/6}Cu_{1/6}Ni_{1/6}Co_{1/6}Fe_{1/6}Mn_{1/6}Ta_2O_{9+\Delta}$ sample depending on the calcination temperature.

Temperature synthesis, °C	Phase composition
650	Ta_2O_5, NiO, Co_3O_4, $Bi_{16}CrO_{27}$, $Bi_{25}FeO_{40}$, $BiTaO_4$, Bi_3TaO_7, pyrochlore
700	Ta_2O_5, NiO, Co_3O_4, $Bi_{16}CrO_{27}$(traces), $BiTaO_4$, pyrochlore
750	Ta_2O_5(traces), NiO, Co_3O_4, Co(Ni)Ta_2O_6, $BiTaO_4$, pyrochlore
800-900	NiO, Co_3O_4, Co(Ni)Ta_2O_6, $BiTaO_4$, pyrochlore
950	Co(Ni)Ta_2O_6, $BiTaO_4$, pyrochlore
1000 –1050	pyrochlore

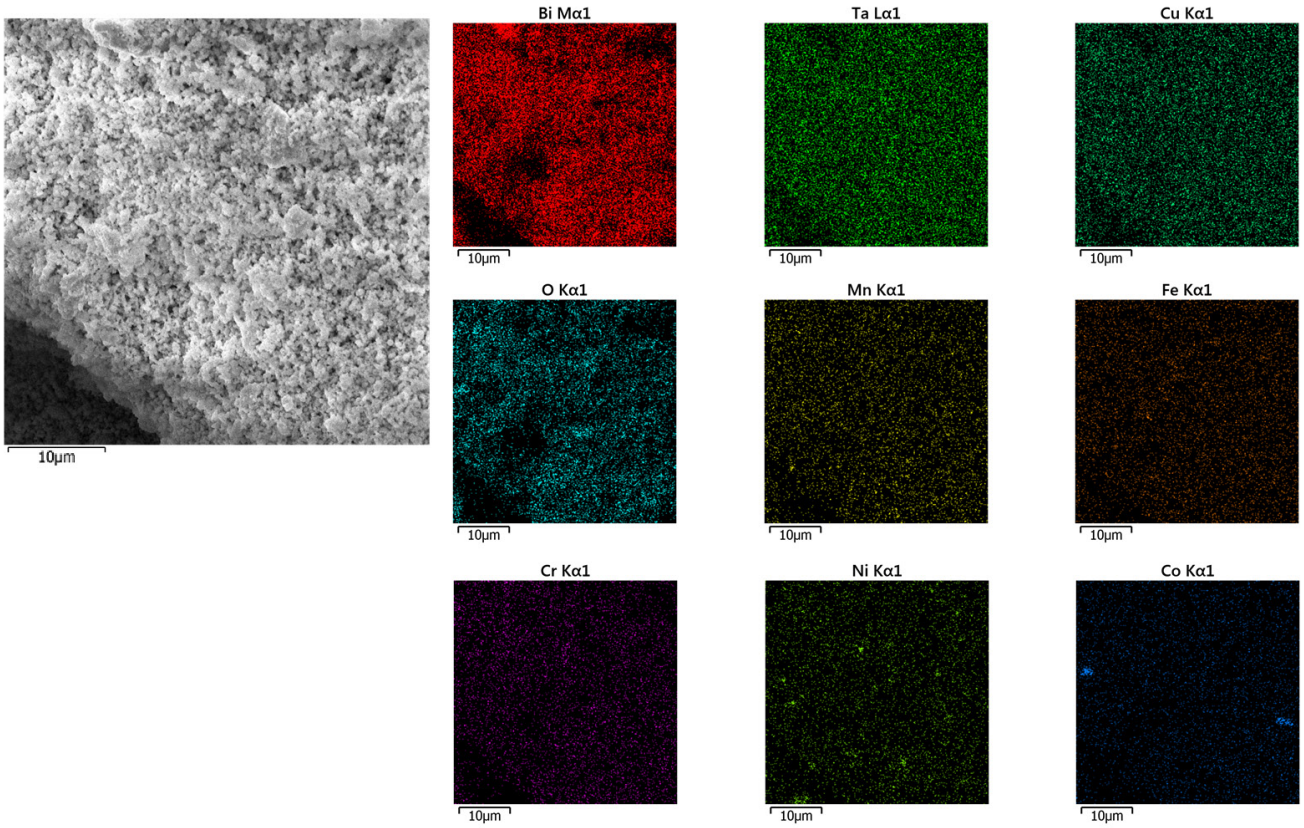

Fig. 2. (Color online) EDS elemental mapping of the $Bi_{2-1/3}Cr_{1/6}Cu_{1/6}Ni_{1/6}Co_{1/6}Fe_{1/6}Mn_{1/6}Ta_2O_{9+\Delta}$ sample, synthesized at 700°C.

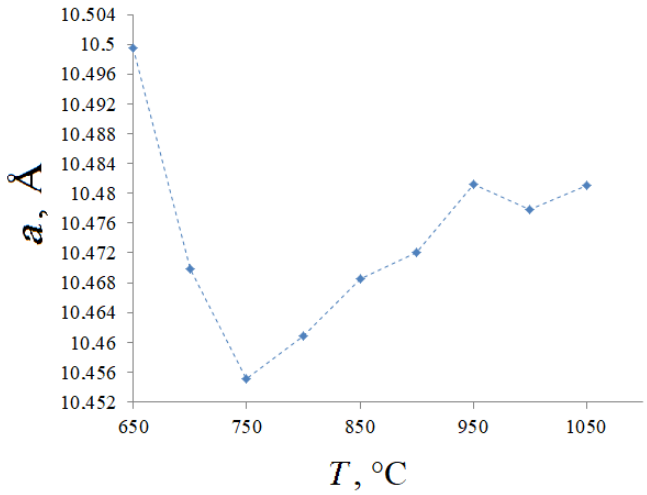

Fig. 3. Change in the unit cell parameter of the pyrochlore phase in the $Bi_{2-1/3}Cr_{1/6}Cu_{1/6}Ni_{1/6}Co_{1/6}Fe_{1/6}Mn_{1/6}Ta_2O_{9+\Delta}$ sample depending on the synthesis temperature.

show a decrease in the intensity of reflections of bismuth orthotantalate. Phase-clean pyrochlore, without admixture of bismuth orthotantalate, is formed at a temperature of 1000–1050°C. Scheme S1 (supplementary material) shows an exemplary route for the synthesis of pyrochlore from precursors.

Figure 3 shows the change in the elementary cell parameter of pyrochlore with an increase in the calcination temperature of the sample. As can be seen from the Fig. 3, the elementary cell parameter changes nonmonotonically during synthesis. It is characteristic that during the synthesis of bismuth orthotantalate (650–750°C), the cell constant of pyrochlore decreases quite sharply with a subsequent increase to a practically constant value a=10.4811 Å at 1050°C. A sharp decrease in the unit cell parameter in the range from 650 to 750°C can be associated with the removal of structural deformation due to the nonstoichiometric composition of low-temperature pyrochlore. The strongly

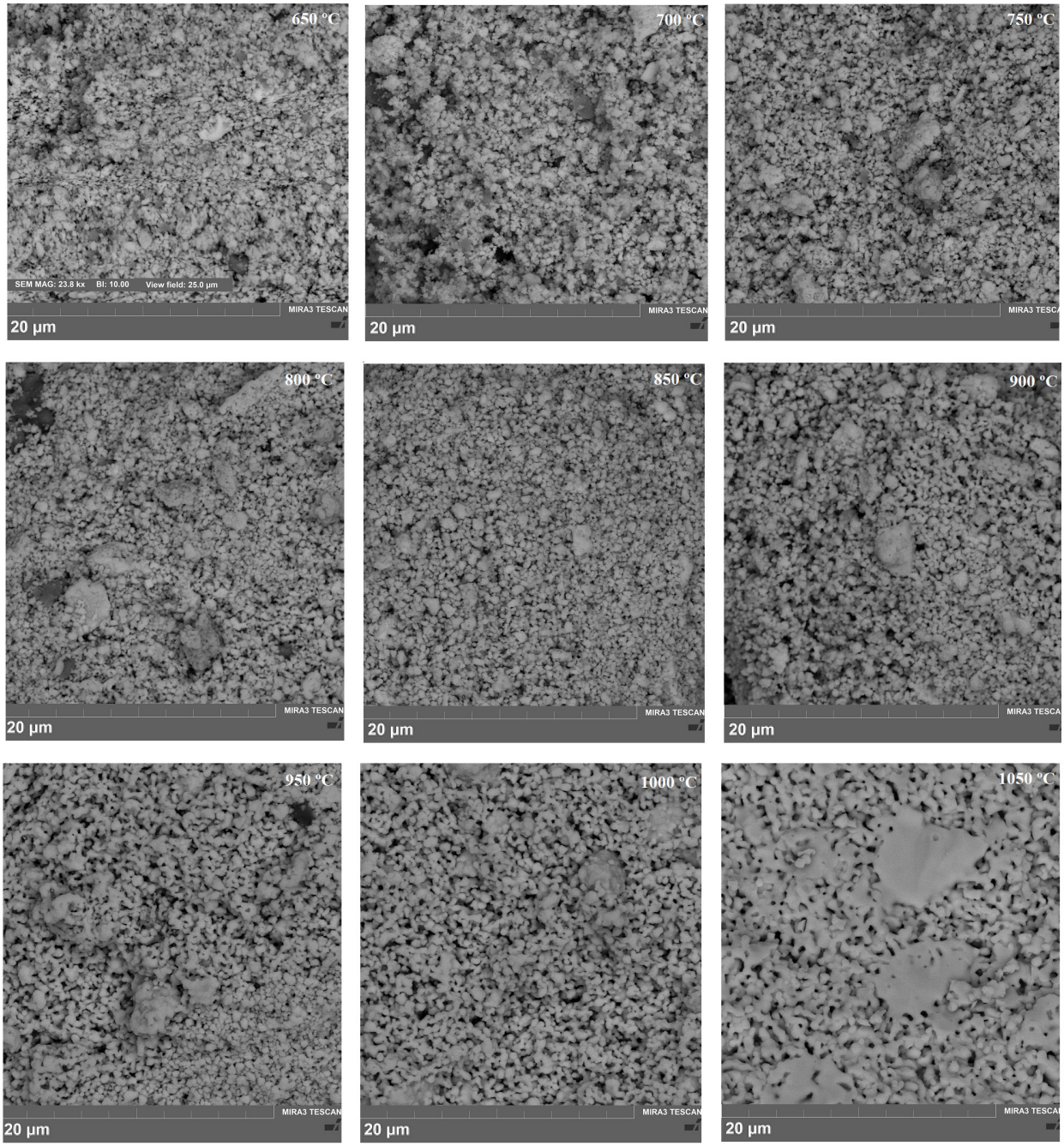

Fig. 4. Surface micrographs of the $Bi_{2-1/3}Cr_{1/6}Cu_{1/6}Ni_{1/6}Co_{1/6}Fe_{1/6}Mn_{1/6}Ta_2O_{9+\Delta}$ samples, synthesized at temperatures from 650 and 1050°C.

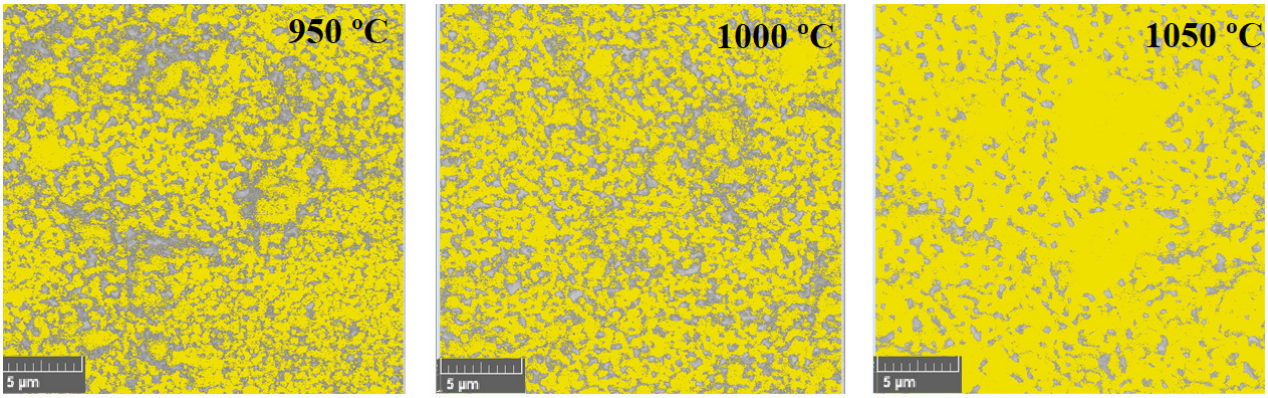

Fig. 5. (Color online) Surface porosity of $Bi_{2-1/3}Cr_{1/6}Cu_{1/6}Ni_{1/6}Co_{1/6}Fe_{1/6}Mn_{1/6}Ta_2O_{9+\Delta}$ samples (pores are gray), calcined at 950, 1000 and 1050°C.

diffuse interference reflections of the pyrochlore phase testify to the high degree of lattice tension. In a similar case, for niobium pyrochlore, in [32], the existence of a pseudoorthorhombic form of pyrochlore was suggested. In our situation, when indexing X-ray patterns, no signs of the presence of a pseudo-orthorhombic modification of pyrochlore were revealed. The gradual increase in the cell constant above 750°C is associated with the inclusion of large cobalt and nickel ions in the crystal structure. Close values of the unit cell parameters of the pyrochlore phase in the range of 1000–1050°C (10.4778 and 10.4811 Å) may indicate the completion of the synthesis process.

Micrographs of the surface of the synthesized $Bi_{2-1/3}Cr_{1/6}Cu_{1/6}Ni_{1/6}Co_{1/6}Fe_{1/6}Mn_{1/6}Ta_2O_{9+\Delta}$ samples in the temperature range 650–1050°C are shown in Fig. 4. An inhomogeneous microstructure with heterogeneous grains and inclusions of impurity phases is typical for samples calcined at a temperature of 650 – 900°C. A porous, dendrite-like microstructure is formed in samples synthesized at a temperature of 950°C and higher. At a temperature of 1050°C, the crystallites are sintered with the formation of monolithic island regions. The longitudinal grain size of ceramics sintered at 1000°C varies in the range of 0.5–1.0 μm.

Grain sintering at 1050°C is confirmed by SEM porosity assessment data. As can be seen from Fig. 5, the porosity of samples calcined at 950, 1000 and 1050°C decreases from 38 to 16%, respectively, which is associated with the formation of a low-porous, monolithic microstructure due to the association of ceramic grains. Thus, the heat treatment temperature of the samples had little effect on the ceramic microstructure.

Apparently, a noticeable association of crystallites should be expected at a temperature close to the melting point of the sample, which is unacceptable because of the threat of loss of composition stoichiometry.

4. Conclusions

High-entropy pyrochlore $Bi_{2-1/3}Cr_{1/6}Mn_{1/6}Fe_{1/6}Co_{1/6}Ni_{1/6}Cu_{1/6}Ta_2O_{9+\Delta}$ (sp. gr. *Fd*-3*m*, a=10.4811 Å) was synthesized by the solid-phase reaction method. Phase-clean pyrochlore was obtained at 1050°C. The microstructure of the sample is porous, loose, formed by partially intergrown grains with an average size of 0.5–1 μm. The process of evolution of the pyrochlore phase is a multi-stage process that ends at a temperature of 1000–1050°C. The precursor of the pyrochlore phase is bismuth orthotantalate, the pyrochlore synthesis reaction consists in the interaction of bismuth orthotantalate with oxides of transition elements. Cobalt and nickel oxides interact at elevated temperatures (850 – 900°C). The oxides $Bi_{16}CrO_{27}$, $Bi_{25}FeO_{40}$, $BiTaO_4$, Bi_3TaO_7, $CoTa_2O_6$ were found as intermediate phases. In the entire studied temperature range, the maximum value of the cell constant is characteristic of nonstoichiometric pyrochlore synthesized at 650°C. Pseudo-orthorhombic modification of pyrochlore was not found.

Supplementary material. *The online version of this paper contains supplementary material available free of charge at the journal's website (lettersonmaterials.com).*

Acknowledgements. The X-ray phase analysis were carried out in the Center for Collective Usage "Geonauka" (Institute of Geology of Komi Science Center of the Ural Branch of the Russian Academy of Sciences).

References

1. S. Murugesan, M.N. Huda, Y. Yan, M.M. Al-Jassim, V. Subramanian. J. Phys. Chem. 114, 10598 (2010). Crossref
2. J. Pandey, V. Shrivastava, R. Nagarajan. Inorg. Chem. 57, 13667 (2018). Crossref
3. C.C. Khaw, K.B. Tan, C.K. Lee. Ceram. Intern. 35, 1473 (2009). Crossref
4. N.A. Zhuk, M.G. Krzhizhanovskaya. Ceram. Int. 47, 30099 (2021). Crossref
5. M.A. Subramanian, G. Aravamudan, G.V. Subba Rao. Prog. Sol. St. Chem. 15, 55 (1983). Crossref
6. R.A. McCauley. J. Appl. Phys. 51, 290 (1980). Crossref
7. T.A. Vanderah, M.W. Lufaso, A.U. Adler, I. Levin, J.C. Nino, V. Provenzano, P.K. Schenck. J. Sol. St. Chem. 179, 3467 (2006). Crossref
8. T.A. Vanderah, T. Siegrist, M.W. Lufaso, M.C. Yeager, R.S. Roth, J.C. Nino, S. Yates. Eur. J. Inorgan. Chem. 2006, 4908 (2006). Crossref
9. M.W. Lufaso, T.A. Vanderah, I.M. Pazos, I. Levin, R.S. Roth, J.C. Nino, V. Provenzano, P.K. Schenck. J. Sol. St. Chem. 179, 3900 (2006). Crossref
10. N.A. Zhuk, M.G. Krzhizhanovskaya, A.V. Koroleva, S.V. Nekipelov, D.V. Sivkov, V.N. Sivkov, A.M. Lebedev, R.G. Chumakov, B.A. Makeev, V.V. Kharton, V.V. Panova, R.I. Korolev. Sol. St. Sci. 125, 106820 (2022). Crossref
11. N.A. Zhuk, M.G. Krzhizhanovskaya, A.V. Koroleva, S.V. Nekipelov, V.V. Kharton, N.A. Sekushin. Inorgan. Chem. 60, 4924 (2021). Crossref
12. M.P. Chon, K.B. Tan, C.C. Khaw, Z. Zainal, Y.H. Taufiq-Yap, S.K. Chen, P.Y. Tan. J. Alloys Comp. 675, 116 (2016). Crossref
13. M. Valant, D. Suvorov. J. Am. Ceram. Soc. 88, 2540 (2005). Crossref
14. F.A. Jusoh, K.B. Tan, Z. Zainal, S.K. Chen, C.C. Khaw, O.J. Lee. J. Mater. Res. Techn. 9, 11022 (2020). Crossref
15. P.Y. Tan, K.B. Tan, C. Khaw, Z. Zainal, S.K. Chen, M.P. Chon. Ceram. Intern. 38, 5401 (2012). Crossref
16. J.C. Nino, M.T. Lanagan, C.A. Randall. J. Appl. Phys. 89, 4512 (2001). Crossref
17. C. Ang, Z. Yu, H.J. Yuon, C.A. Randall. Appl. Phys. Lett. 80, 4807 (2002). Crossref
18. S. Kamba, V. Porokhovskyy, A. Pashkin. Phys. Rev. B: Condens. Matter. 66, 1 (2002). Crossref
19. M. Valant. J. Am. Ceram. Soc. 92, 955 (2009). Crossref
20. N.A. Zhuk, M.G. Krzhizhanovskaya, A.V. Koroleva, N.A. Sekushin, S.V. Nekipelov, V.V. Kharton, B.A. Makeev, V.P. Lutoev, Y.D. Sennikova. Inorg. Chem. 61, 4270 (2022). Crossref
21. N.A. Zhuk, N.A. Sekushin, M.G. Krzhizhanovskaya, V.V. Kharton. Sol. St. Ion. 377, 115868 (2022). Crossref
22. N.A. Zhuk, M.G. Krzhizhanovskaya, A.V. Koroleva, A.A. Reveguk, D.V. Sivkov, S.V. Nekipelov. Ceram. Intern. 48, 14849 (2022). Crossref

23. Ismunandar, T. Kamiyama, K. Oikawa, A. Hoshikawa, B. J. Kennedy, Y. Kubota, K. Kato. Mater. Res. Bull. 39, 553 (2004). Crossref
24. L. G. Akselrud, Yu. N. Grin, P. Yu. Zavalij, et al. CSD-universal program package for single crystal or powder structure data treatment. Thes. Rep. XII Eur. Crystallogr. Meet. (1989) p. 155.
25. N. A. Zhuk, M. G. Krzhizhanovskaya, V. A. Belyy, V. V. Kharton, A. I. Chichineva. Chem. Mater. 32, 5493 (2020). Crossref
26. X. Zhou, J. Yan, G. Wang, S. Wang, L. Liu, G. Shu. Can. Mineral. 35, 35 (1997).
27. D. C. Craid, N. C. Stephenson. J. Sol. St. Chem. 15, 1 (1975). Crossref
28. A. Maitre, M. Francois, J. C. Gachon. J. Phase Equilibria and Diffusion. 25, 59 (2004). Crossref
29. M. Struzik, X. Liu, I. Abrahams, F. Krok, M. Malys, J. R. Dygas. Solid State Ionics. 218, 25 (2012). Crossref
30. G. Gattow, D. Schultze. Bismuth Oxides: VI. Anorg. Allg. Chem. 328, 44 (1964).
31. V. A. Murav'ev, B. A. Makeev, M. G. Krzhizhanovskaya, R. I. Korolev, N. A. Zhuk. Glass Ceram. 79, 70 (2022). Crossref
32. J. C. Nino, M. T. Lanagan, C. A. Randall. J. Mater. Res. 16, 1460 (2001). Crossref